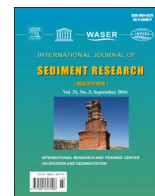




ELSEVIER

Contents lists available at ScienceDirect

International Journal of Sediment Research

journal homepage: www.elsevier.com/locate/ijsrc

Experimental study of bed-load transport using particle motion tracking

Jaeho Shim, Jennifer G. Duan*

Department of Civil Engineering and Engineering Mechanics, University of Arizona, Tucson, AZ 85721, USA

ARTICLE INFO

Article history:

Received 22 September 2015

Received in revised form

17 October 2016

Accepted 21 October 2016

Keywords:

Bed-load transport

Particle tracking

Particle velocity

ABSTRACT

A series of experiments were conducted in a flume to study bed-load transport. The motion of bed-load particles was captured by a series of images taken by a high-speed camera. A novel particle motion tracking method was developed to automatically detect all the moving particles and calculate the instantaneous particle velocities. The instantaneous bed load transport rate was calculated based on particle velocity and the volume of moving particles. To verify this method, bed load transport rate based on the image processing technique was compared to the manually measured ones as well as data from other experiments. Results showed that the new technique made it possible to quantify the spatial and temporal variations of bed load transport rate at the individual particle scale.

© 2016 International Research and Training Centre on Erosion and Sedimentation/the World Association for Sedimentation and Erosion Research. Published by Elsevier B.V. All rights reserved.

1. Introduction

Accurately calculating bed load transport rates has been a challenge in hydraulic engineering for decades. Bed load transport depends on the interaction between flow and sediment particles (Bridge & Dominic, 1984). Determining the velocity of sediment particles on a river bed is essential to quantify the transport rate. Many researchers (Bridge & Dominic, 1984; Francis, 1973; Lee & Hsu, 1994; Niño & García, 1994a; Novak & Nalluri, 1975; Sekine & Kikkawa, 1992) have studied the characteristics of particle motion and velocity. For example, images from high-speed cameras have enabled the accurate measurement of individual sediment motion (Francis, 1973; Furbish et al., 2012; Houssais & Lajeunesse, 2012; Lajeunesse et al., 2010; Lee & Hsu, 1994; Niño & García, 1994b).

Advances in image processing techniques have permitted the continuous, multiple detections of moving particles, and also the automatic processing of captured images. For example, using consecutive images, fractional mobility of sediment particles was obtained by overlapping images of bed surface and identifying the sediments that remained immobile (Wu & Yang, 2004). Two particle motion tracking techniques, Eulerian (Radice et al., 2006) and Lagrangian frameworks (Heays et al., 2014; Houssais & Lajeunesse, 2012; Lajeunesse et al., 2010), are commonly used. Radice et al.

(2006) used Eulerian framework, the Particle Image Velocimetry (PIV) technique, to measure the moving particle velocity. Eulerian technique is effective for detecting multiple moving particles. However, it is not suitable for tracking the motion of an individual particle. Lajeunesse et al. (2010) and Houssais and Lajeunesse (2012) used Lagrangian framework, Particle Tracking Velocimetry (PTV) to investigate the average velocity, density, and transport rate of moving particles. The PTV technique was also applied in a series of experiments using colored particles transported over fixed bed (Campagnol et al., 2013; Heays et al., 2014; Papanicolaou et al., 1999). However, due to large volumes of images, some researchers have chosen to analyze only the pre-colored particles, and others only selected representative images for manual processing.

Bed-load sediment moves along river bed by sliding, rolling, and saltating. Among them, saltating motion is dominant at high transport rate. Researchers (Bridge & Dominic, 1984; Fernandez Luque & Van Beek, 1976; Niño & García, 1994a) have used the trajectory of saltating particles to determine its velocity. These experiments were conducted either on fixed or mobile bed, and high-speed camera was employed to capture the images. Due to the limitation of the camera and also the image processing technique, it's difficult to automatically distinguish and measure all the moving particles, so that only recognizable individual particle (e.g. saltating particles) was measured. From these limited experimental datasets, empirical equations of bed load transport were formulated primarily based on the measurements of saltating

* Corresponding author.

E-mail addresses: jaeho@email.arizona.edu (J. Shim), gduan@email.arizona.edu (J.G. Duan).

<http://dx.doi.org/10.1016/j.ijsrc.2016.10.002>

1001-6279/© 2016 International Research and Training Centre on Erosion and Sedimentation/the World Association for Sedimentation and Erosion Research. Published by Elsevier B.V. All rights reserved.

Nomenclature

A_i^n	Area of the i th contour (m^2);	u_{pi}, u_{xi}, u_{yi}	Instantaneous, streamwise and transverse velocity of i th particle (ms^{-1});
A_s	Surface area covered in the image (m^2)	$\bar{u}_p, \bar{u}_x, \bar{u}_y$	Time-averaged particle velocity, and its components instreamwise and transverse directions, respectively (ms^{-1});
D	Diameter of sediment particle (m)	u_*	Shear velocity (ms^{-1});
D_i	Diameter of i th sediment particle (m);	u_{*p}	Dimensionless instantaneous particle velocity (-)
d_{16}, d_{50}, d_{84}	Grain diameter for which 16%, 50% and 84% are finer, respectively (m);	V_s	Velocity scale (ms^{-1})
g	Acceleration of gravity (ms^{-2})	w	Width of test area (m);
k_s	Size of bed roughness (m)	α, β	Shape and scale parameter, respectively;
L	Particle moving length (m)	γ, γ_s	Specific weight of water and sediment, respectively (Nm^{-3});
N	Number of total frames.	θ	Orientation angle of particle motion ($^\circ$)
n	Number of moving particles in the frame	ν	Kinematic viscosity of water (m^2s^{-1})
q_b	Bed-load transport rate per unit width ($kgm^{-1}s^{-1}$);	ρ, ρ_s	Density of water and sediment, respectively (kgm^{-3});
q_{bn}	Sediment transport rate per unit width at the n th frame ($kgm^{-1}s^{-1}$);	σ	Standard deviation of particle velocity (ms^{-1});
R	Hydraulic radius (m);	σ_g	Standard deviation of sediment particle size (m);
Re_*	Particle Reynolds number (-);	τ	Bed shear stress (Nm^{-2});
S	Bed slope (-);	τ_c	Critical bed shear stress (Nm^{-2});
SG	Specific gravity (-);	τ_*	Shields number of sediment particle (-);
T_*	Dimensionless travel time (-);	τ_{*c}	Critical Shields number of sediment particle (-);
\bar{T}	Mean travel time (s);	Φ	Dimensionless sediment transport rate (-);
u_p, u_x, u_y	Instantaneous, streamwise and transverse particle velocity (ms^{-1});	V_i	Volume of the i th particle at each frame (m^3);

particles (Abbott & Francis, 1977; Bagnold, 1973; Francis, 1973; Lee & Hsu, 1994; Niño & García, 1994b). Because of this, rolling and sliding particles are often neglected, even though rolling particles can contribute significantly to bed load transport (Drake et al., 1988; Julien & Bounvilay, 2013). The number of moving particles in a given flow condition was not measured as well. Consequently, the resulting bed load transport equations are not an accurate representation of all the moving sediment. Recently, Papanicolaou et al. (2002) and Ramesh et al. (2011) investigated bed load transport having both rolling and saltation particles. Ramesh et al. (2011) also derived an empirical relation for rolling or saltating particles using the dimensionless flow and particle velocity parameters in Sekine and Kikkawa (1992). Tregnaghi et al. (2012a) found, at the incipient particle motion, the fluctuation of fluid force, grain resistance, and geometrical configuration of mobile bed surface are the key factors for determining particle velocity. However, those studies did not count all the moving particles, but only selected particles for image processing. Recent studies (Furbish et al., 2012; Roseberry et al., 2012) applied an imaging technology (ImageJ) to measure bed-load particle transport, and derived a probabilistic model for particle transport in turbulent flow. Their results showed that the distribution of particle velocity satisfies an exponential distribution. Ancey and Heyman (2014) applied a stochastic model to analyze bed load motions and concluded the fluctuations in the number of moving particles are Poisson at low shear stress, but depart from the Exner equation at high shear stress. Conclusions from those studies regarding particle velocity and its statistical properties require additional independent verifications, and the correlations between particle transport properties and bed load transport rate also need to be explored further.

This study aims to apply a newly developed particle tracking method to accurately measure the velocities of all the moving bed load particles at various flow conditions. The study selected flow conditions and sediment particles where both rolling and saltating motions are present. The novel particle tracking method is capable of tracking all of the moving sediment particles on a bed surface without pre-coloring or isolating particles, and was programmed

in C++ language using OPEN-CV library. This complete measurement of particle velocity field enables us to study bed load transport at the particle scale. Both the mean bed load transport rate, as well as the deviation of bed load transport rate were obtained from these measurements. These data supplemented the data from Roseberry et al. (2012), Recking et al. (2008) at low shear stress, and evaluated the exponential-like PDFs for the streamwise and transverse particle velocities. In the following sections, the experimental set-up, data processing technique, experimental result, and conclusion are presented in sequence.

2. Experimental setup

2.1. Flume setup

The experiments were conducted in a rectangular titling flume, which is 0.15 m wide, and 2.4 m long. The side wall was made of Plexiglas, and its roughness is negligible compared to the roughness on a mobile bed surface. Bed slope was measured using a digital inclinometer with an accuracy of 0.1° . The incoming flow was pumped into the channel at constant discharges from a large water tank, and controlled by a valve on the pipe. A honeycomb metal sheet was placed at the inlet to stabilize flow at the entrance. The measurement section is 0.12 m long, and located at 1.7 m away from the flume entrance. The bottom of the flume was covered by 5 cm deep uniformly sized sediment. This study used two groups of uniform sediment with median sizes of 1.5 mm and 2.4 mm, respectively (Table 1). The density of sediment is $\rho_s = 2650 \text{ kg/m}^3$. The standard deviations of sediment mixture, $\sigma_g = (d_{84}/d_{16})^{0.5}$, are 1.225 and 1.296, respectively. Sediment mixture with the value of σ_g less than 1.6 can be considered as uniform (Parker, 2008). During the experiment, sediment was fed into the flume externally at the entrance to ensure steady uniform flow condition. The feeding rate is approximately the transport rate we measured at the end of the flume. This is achieved by using all the sediment collected at the flume end. A total of 24 experimental runs were performed, and over 20,000 instantaneous particle velocities in the horizontal plane were measured. Those

Table 1
Characteristics of sediments used in experiments.

Case	D_{50} (m)	Q (m^3s^{-1})	S	τ_* (Nm^{-2})	u_* (ms^{-1})	σ_g	Re_*	ρ_s (kgm^{-3})	H (m)
1	0.0015	0.00048–0.00164	0.0078–0.0227	0.069–0.113	0.045–0.057	1.225	90–144	2650	0.02–0.035
2	0.0024	0.00056–0.00172	0.0061–0.0236	0.037–0.093	0.038–0.060	1.296	108–138	2650	0.03–0.037

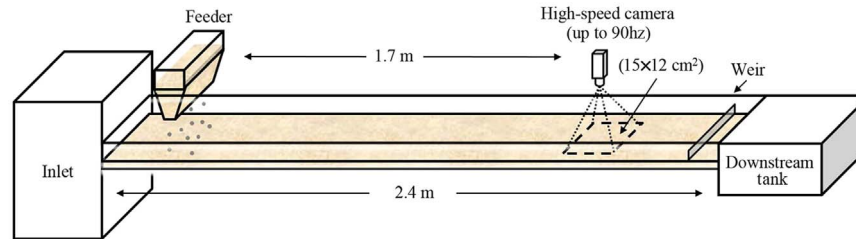


Fig. 1. Schematic of experimental setup.

measurements were used to calculate the mean and standard deviation of particle velocities. A schematic experimental setup is shown in Fig. 1.

2.2. Hydraulic and sediment transport parameters and conditions

In each experiment, flow discharge was constant. There is a flat panel at the exit to regulate the water level. Without this panel, flow depth is critical at the exit. As the panel being raised slightly, a reach of uniform flow was observed in the flume. When water depths measured at five different locations along the flume were within 1 mm difference, the flow was treated as uniform. The streamwise bed shear stress, τ , is then approximated by

$$\tau = \rho g R S \quad (1)$$

where ρ is water density, g is the acceleration of gravity, R is hydraulic radius, and S is bed slope. The Shields number, τ_* , and the shear velocity are given by

$$\tau_* = \frac{\tau}{g(\rho_s - \rho)D} \quad (2)$$

$$u_* = \sqrt{\frac{\tau}{\rho}} = \sqrt{gRS} \quad (3)$$

where D is the size of sediment particle, and u_* is the friction velocity. Flow parameters and sediment characteristics for all the runs are summarized in Table 1. The critical shear stress was calculated as $\tau_{*c} = \tau_{*c}(\gamma_s - \gamma)d_{50}$, in which γ_s , γ are the specific weight of sediment and water, respectively. A constant value of critical Shields number, $\tau_{*c} = 0.031$, for Re_* ranging from 90 to 150, was used in this study (Buffington & Montgomery, 1997). The thickness of viscous sublayer relative to that of the boundary roughness height determines if flow is hydraulic smooth, transitional, or rough (Le Roux, 2004). To distinguish different types of flow, the particle Reynolds number Re_* is calculated as:

$$\text{Re}_* = u_* k_s / \nu \quad (4)$$

where k_s is the size of bed roughness, and ν is kinematic viscosity. When Re_* is less than 5, flow is smooth; and Re_* is greater than 60, it is rough. The transitional flow has Re_* between 5 and 60. In this study, the particle Reynolds number Re_* ranges from 90 to 150. Therefore, all the runs were conducted in the rough flow regime. For each run, the dimensionless bed load transport rate, Φ was calculated as:

$$\Phi = \frac{q_b}{\sqrt{(SG - 1)gD^3}} \quad (5)$$

where q_b is bed-load transport rate, $SG = \rho_s/\rho$, is the specific gravity.

2.3. Camera system setup

The motions of sediment particles were captured by a high-speed digital camera (Sony XCD-V60). The camera can achieve up to 120 frames per second (fps) with a resolution of 640×480 pixels. This camera was mounted on a rod, and placed vertically just above the water surface. The rod was clamped to the flume so that they would incline together at the same angle. A small flat transparent plastic plate was placed on the water surface to remove image distortions caused by the light refraction from water-surface fluctuations. This placement ensures the camera has a clear view of the moving particles. To minimize the effects of pressurization caused by local contraction surface, the plastic plate was very thin that can float freely right on the flow surface without imposing any force. Although the plastic plate does not impose any pressure force, there is minimal friction force on the water surface. The ratio of particle size to flow depth is from 3.7% to 8%. This minor friction effect was assumed to be negligible in this study, which needs to be noticed by other researchers interested in the data.

The camera was connected to and controlled by a computer, and automatically transferred captured images to the computer hard drive. Preliminary tests showed that the best image quality was achieved at a frame rate of 90 fps, suitable for capturing clear particle motion pictures. The minimum number of pixels for one sediment particle area is approximately 30, which is the threshold pixel size for determining the size and location of a particle. The test duration for each run was typically 16 s, but varied by the frame rate. In this study, over 1300 consecutive images were captured during each run at the frame rate of 90 fps. To ensure the captured images are representative, 3–5 series of images was captured for each run. In the image analysis, if two or more series yielded the same results of particle velocity and deviation, one series was selected as the representation of the experimental run. If none of the series replicated the other, this run failed, and the data was not used.

3. Particle motion tracking

This study developed a particle tracking method that is able to automatically identify moving particles, match them in consecutive images, and compute particle velocity and bed load transport rate. This automation of particle velocity measurements consists of three

major steps: 1) detecting moving particles through background image subtraction, 2) transforming images using morphological processes, and 3) tracking particles by moving distance, contour area, and color histogram.

3.1. Image processing

The OpenCV library (<http://code.opencv.org>), a collection of computer graphics functions written in C++, was used for the image processing workflow programming. At first, the captured digital images were converted to binary images. Secondly, each image was subtracted from the background image taken when the bed was still. The remains from the subtraction are the particles being moved by flow (Bradski & Kaehler, 2008). Consequently, all the moving particles were isolated and identified in each image. Thirdly, morphologic erosion and dilation transformations were applied to identify each moving particle with a distinct shape. Erosion and dilation are the most fundamental morphological transformation processes for removing noise, finding holes, isolating individual elements, and jointing disparate elements in the image. The erosion process removes the noise, such as very small motion of debris, and the dilation process was applied to fill some of the holes (e.g., empty pixels) inside the defined moving particles (Laganier, 2011). As a consequence, a binary image having the edges of all the moving particles was obtained. The contour line (outline) of a moving particle is obtained by connecting the edge pixels of a particle. The locations of moving particles (x and y coordinates) were calculated as the geometric centers of those contours. Fourthly, the images having the contours of moving particles were then overlapped on the original image as shown in Fig. 2. This overlap recognizes the moving particles in the original image. The surface fraction of moving particles is then calculated as the fraction of the contour covered area in the image. Through those four processes, we obtained the location, size, and shape of all the moving particles in each image.

3.2. Particle motion tracking algorithm

To track particle's trajectory, some researchers used a minimal distance to find the best particle location (Campagnol et al., 2013; Frey, 2014), others used the similarity of surface area, the ratio between the surface area of a particle in two consecutive images, to locate the identical particle (Heays et al., 2014). In the present study, we applied several criteria to the subtracted images for tracking the particle. In the first image, each particle is tagged with a unique ID number. Then, a searching area (SA) for each particle was defined based on the maximum possible displacement in x- and y-directions, which is the product of the maximum flow velocity and the time interval between two images. The searching

area has to be sufficiently large to encompass the trajectory of the fastest moving particle. In the consecutive image, if only one particle appeared in the SA, this particle is the new location of the tagged particle. If more than one particle were identified in the SA, three criteria were used to search for the tagged one. The first criterion is to measure the distances between the tagged particle in the starting image and all the other particles in the consecutive image within the SA. The particle that has the minimum distance is the new location of the tagged particle. This criterion is suitable for tracking sparse moving particles at low bed load transport rate. Another criterion is to compare the ratios of surface area of each particle in the SA to that of the tagged particle. The particle having the ratio nearly equal to 1.0 is the new location of the tagged one. The third criterion is the color morphology within each particle contour. By overlapping the start and the consecutive images, the histograms of color values within the contour of the tagged particle and the captured ones in the SA were extracted. The tracking particle should have the best match of the color histogram with the tagged one. Those criteria were applied together to search for the tagged particle in the consecutive image. Ideally, all three search criteria need to be satisfied to confirm the new location of the tagged particle. In some cases, particularly, high transport rate, only two criteria were met for some particles.

Each particle has a unique ID number in the first image in which it appears. The same ID number was kept for the same particle in all the images allowing for the trajectory of each moving particle to be obtained by connecting the particle centers with the same ID number. The instantaneous particle velocity was calculated using the distance that the center of a particle had travelled in two consecutive images. According to the direction of particle motion, the total velocity was decomposed into the streamwise and transverse velocity. The entire image processing procedure was programmed by using the C++ language and OpenCV graphics library. The particle tracking algorithm was able to automatically distinguish multiple moving particles and track the motion of each particle on mobile bed surface. This provided sufficient data for calculating the statistical properties of bed-load particle velocity and transport rate.

4. Experimental results

4.1. Accuracy of particle tracking

In order to verify the accuracy of measured particle velocity and sediment transport rate using our particle tracking method, 100 consecutive images were processed, and the manually obtained particle velocity and sediment transport rate were compared with the computer processed ones. At first the number of moving particle in

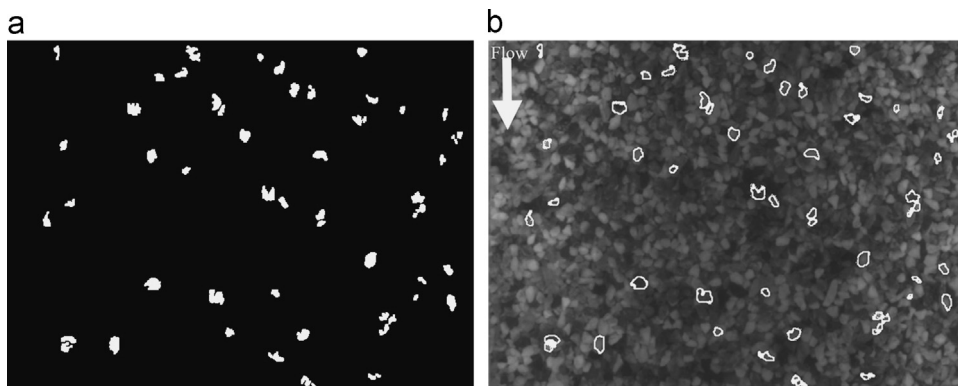


Fig. 2. Moving particle contour overlapped with original image.

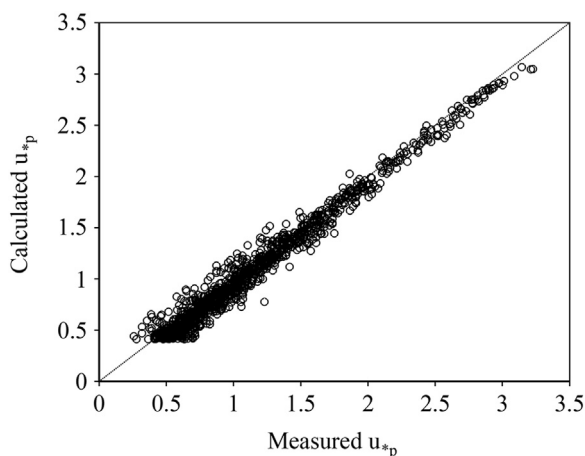


Fig. 3. Calculated dimensionless particle velocity versus the manually measured.

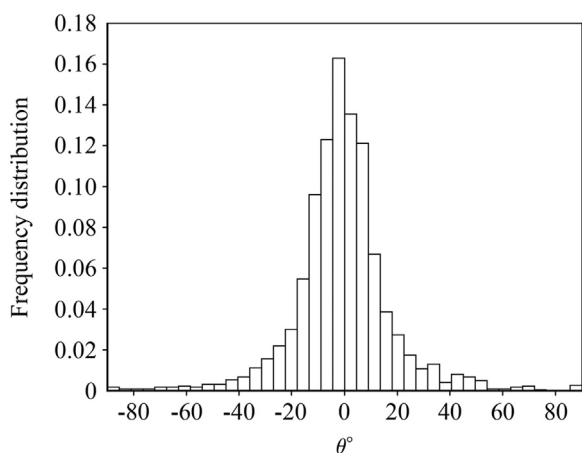


Fig. 4. Frequency distribution of orientation angle.

each image were manually counted, and then were matched with identical particles from different images. Results showed that the number of particles detected by the particle tracking algorithm is 93%. Some moving particles were missed because the particles were too small, or two particles were too close to separate in the automated procedure. The instantaneous velocities were also manually calculated using consecutive images. The distance travelled by one particle in two consecutive images was manually measured by a fine scaled ruler (1 mm accuracy). The instantaneous particle velocity, denoted by u_p , was calculated by dividing this distance by the time period between two frames. A velocity scale, $V_s = \sqrt{(SG-1)gD}$, is used to non-dimensionalize the instantaneous particle velocity. These manually calculated velocities were compared with those determined from the particle motion tracking in Fig. 3, where $u_{sp} = u_p/V_s$. Results from both methods matched very well.

4.2. Instantaneous particle velocity

The direction of particle motion was characterized by the orientation angle, θ , defined as $\tan^{-1}(u_{yi}/u_{xi})$, where u_{xi} and u_{yi} are the i th particle velocities in the streamwise and transverse directions, respectively. Fig. 4 is the frequency distribution of orientation angles, and shows that the direction of particle motion was nearly in the streamwise direction ($\tan \theta = 0$). In addition, the trajectories of several moving particles in ten successive images are illustrated in Fig. 5, where the arrows indicate the exact directions of moving particles. The time interval between two consecutive frames is 1/90 s. It was noticed that the tracking

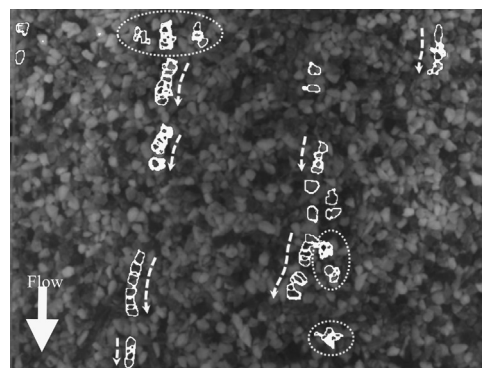


Fig. 5. Trajectories of moving particles for the particle size of 2.4 mm (Case 2); the number of frame is 10 consecutive images. The arrow shows the trajectories of moving particles, and the circle area indicates shaking particles.

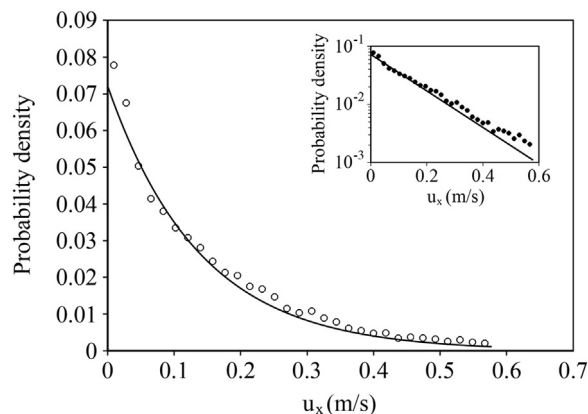


Fig. 6. Probability density function of streamwise particle velocity u_x (m/s) with the particle size of 2.4 mm. Exponential PDF: circles are experiment data. Solid line represents exponential distribution by Eq. (6).

algorithm successfully detected nearly all the moving particles including those having very minor displacements, typically less than the particle diameter. These particles of minor displacement are called the shaking particles that do not move down the channel, but re-adjust their positions according to the surrounding flow field. If the shaking particles are included, the spatially and temporally averaged particle velocity will be artificially reduced. To avoid this, a cutoff distance was set to exclude those particles for the velocity and transport rate calculation. The cutoff distance was about 0.4–0.7 mm depending on the particle size and flow velocity.

Experimental research (Furbish et al., 2012; Furbish & Schmeckle, 2013; Heays et al., 2014; Lajeunesse et al., 2010) has found that the probability density function (PDF) for the streamwise particle velocity is an exponential distribution, and that the PDF for the transverse particle velocity is a normal distribution with zero mean value, $\bar{u}_y = 0$. Experimental results from this study showed that the PDF of streamwise particle velocity are close to the exponential distribution (Fig. 6) as observed in Lajeunesse et al. (2010) and Roseberry et al. (2012). The probability density function is written as:

$$f(u_x) = \frac{1}{\bar{u}_x} e^{-u_x/\bar{u}_x} \quad (6)$$

where \bar{u}_x is the average streamwise particle velocity. Eq. (6) slightly underestimated the experimental data at high particle velocity as shown in Fig. 6. However, it's the best fitting curve we can find to match the observed data. This also confirms similar results from other researches (Furbish et al., 2012; Lajeunesse et al.,

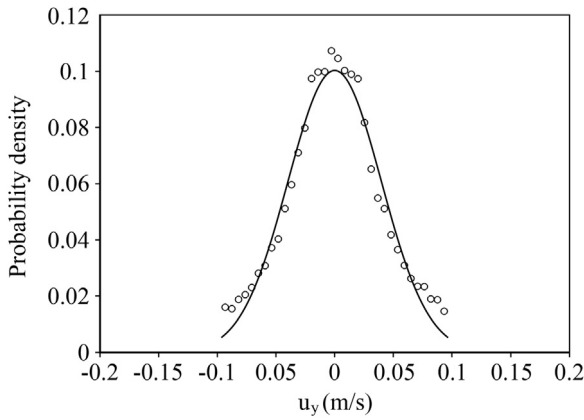


Fig. 7. Gaussian PDF of transverse particle velocity with the particle size of 2.4 mm. Circles are experiment data. Solid line represents Gaussian distribution by Eq. (7).

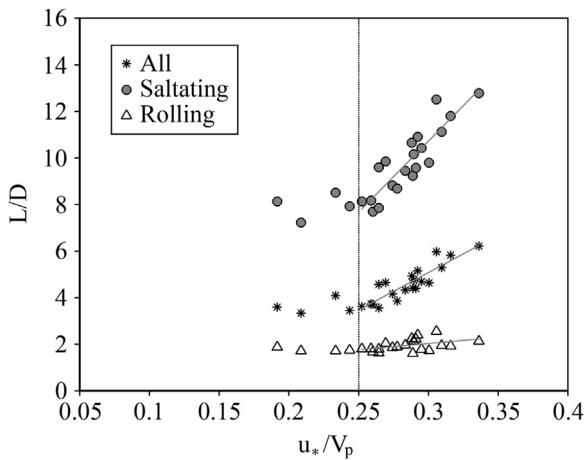


Fig. 8. Travel length of moving particle; all of moving particles, saltating and rolling.

2010; Roseberry et al., 2012). The PDF of the transverse particle velocity is approximated by the Gaussian distribution as shown in Fig. 7.

$$f(u_y) = \frac{1}{\sigma\sqrt{2\pi}} e^{-((u_y - \bar{u}_y)/2\sigma)^2} \quad (7)$$

where σ is the standard deviation of transverse particle velocity, and \bar{u}_y is the average transverse particle velocity. Although the Gaussian distribution matched the peak values very well, it underestimated the measurements at both tails.

4.3. Travel length and time

For each run, we measured all of the moving particles trajectories, including sliding, rolling, and saltating ones, with our particle tracking program. From those trajectories, we measured the travel length and time of all the moving particles. In Fig. 8, we plot the correlation between average L/D and u_* / V_s (the middle line). At low shear velocity ($u_* / V_s < 0.25$) the particle travel length is approximately a constant, 4.0. However, when the non-dimensional shear velocity is greater than 0.25, the travel length increases rapidly with the shear stress. This means when sliding/rolling motion is dominant at low shear velocity, the average particle travel length is about four times the particle size. As the shear stress increases, the saltating motion becomes dominant, and the particle travel length increases with the shearing stress shown in Fig. 8 (the middle line). The empirical relations for the

particle travel length are formulated as:

$$L/D \approx 4 u_* / V_s < 0.25 \quad (8)$$

$$L/D = 32.2(u_* / V_s) - 4.5792 u_* / V_s \geq 0.25 \quad (9)$$

It is known the travel length and time of a saltation motion is much greater than those of a sliding/rolling one. To separate the saltation motion from the sliding/rolling motions, the minimum distance of saltation motion and the maximum distance of sliding/rolling motions need to be defined. The experimental data showed two distinct regions of particle travel distance: one is above 7D, and the other is less than 3D. Over 80% of particles are resided in those two regions. Therefore, it is assumed a saltating motion travels at least 7D continuously, while a rolling/sliding motion travels less than 3D in a continuous motion. This differentiation of the saltating and rolling/sliding motion using the travel length is similar to those (Lee & Hsu, 1994; Niño & García, 1998) observed, but requires further laboratory verification. Based on this, the travel length and time for the saltation and rolling/sliding motions were calculated. The ratio of an identical particle surface area in two consecutive images is defined as A_i^n / A_i^{n+1} , where i is particle ID, and n is n th of frame, is between 0.5 and 1.5. Then, it is considered as a saltating motion. Travel lengths for sliding/rolling and saltation particles, L/D , were constants, 2 and 8, respectively, when $u_* / V_s < 0.25$. When $u_* / V_s \geq 0.25$, the travel length linearly increased with the shear velocity. However, the linear relations for saltation and rolling/sliding motions are different. The empirical formulated equations are listed below:

For the saltating particles (Fig. 8 – the upper line):

$$L/D \approx 8 u_* / V_s < 0.25 \quad (10)$$

$$L/D = 60.967(u_* / V_s) - 7.563 u_* / V_s \geq 0.25 \quad (11)$$

For the sliding/rolling particles (Fig. 8 – the lower line):

$$L/D \approx 2 u_* / V_s < 0.25 \quad (12)$$

$$L/D = 5.3848(u_* / V_s) + 0.4182 u_* / V_s \geq 0.25 \quad (13)$$

In addition, the probability density function (PDF) of the travel lengths for all the moving particles, the sliding/rolling ones, and the saltating ones were plotted in Figs. 9a, b, and c, respectively. Experimental results showed that the PDFs for the travel length (L/D) of both the saltating and sliding/rolling particles satisfy the Gamma distribution.

$$P(L/D) = \frac{L/D^\alpha}{\Gamma(\alpha+1)\beta^{\alpha+1}} e^{-(L/D)/\beta} \quad (14)$$

where α and β are the shape and scale parameters with $\alpha > 0$ and $\beta > 0$, and Γ is the gamma function. In Fig. 9, for the PDF of saltating and rolling/sliding particles, the peak value of saltating travel length is about 10D, while the peak value for sliding/rolling particles is much less, about 2D.

The mean travel time, \bar{T} , normalized by the characteristic settling time as $T_* = \bar{T} / \sqrt{D/Rg}$, is shown in Fig. 10. The averaged dimensionless travel time, T_* , is nearly a constant for all the particles (Eq. 15), with saltating particles traveling about twice as long as those with shorten travel distances (Eq. 16). Eq. (17) is the dimensionless travel time for the rolling/sliding particles.

$$\bar{T} / \sqrt{D/Rg} = 4.8 \pm 0.6 \text{ All of particle} \quad (15)$$

$$\bar{T} / \sqrt{D/Rg} = 10.6 \pm 1.0 \text{ Saltating particle} \quad (16)$$

$$\bar{T} / \sqrt{D/Rg} = 2.43 \pm 0.25 \text{ Rolling particle} \quad (17)$$

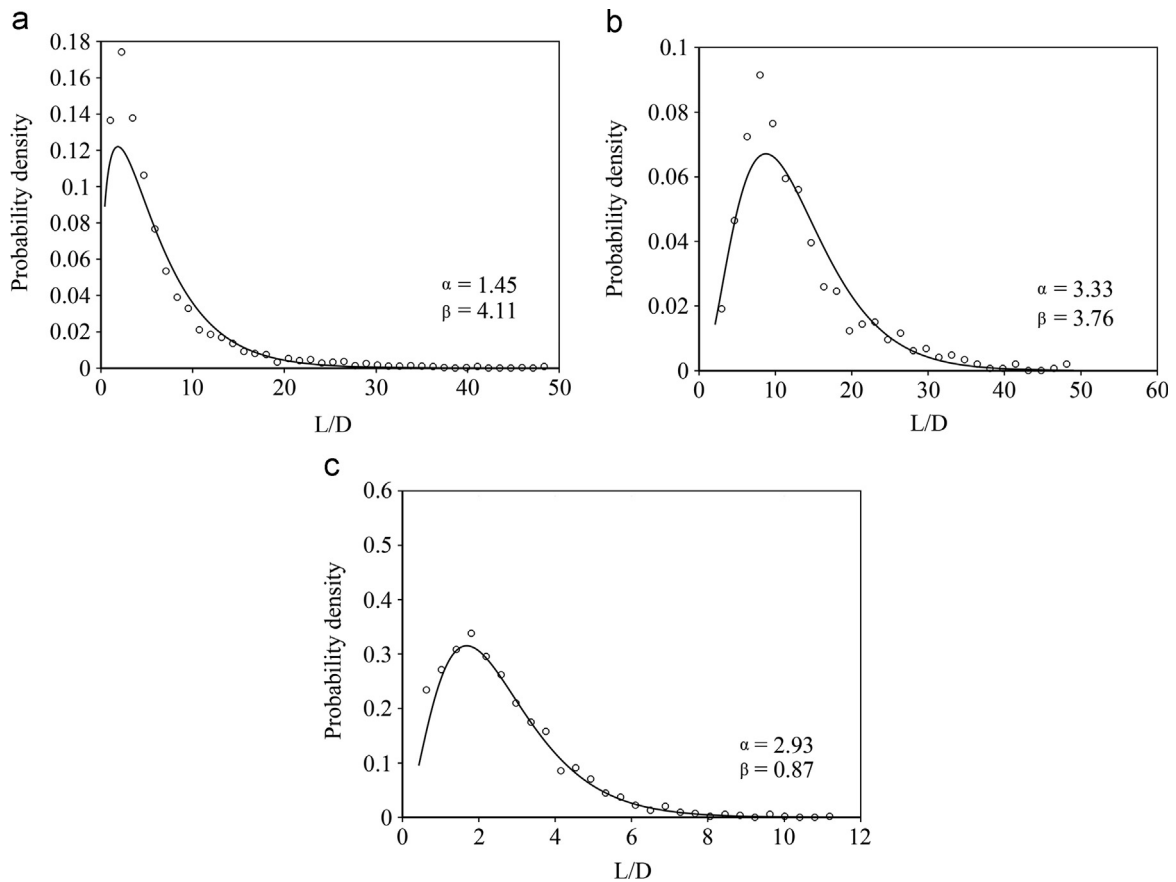


Fig. 9. Gamma PDF of the travel length: (a) all of moving particles ($\alpha=1.45$, $\beta=4.11$ for 2.4 mm) (b) saltating particles (shape and scale parameter for gamma PDF: $\alpha=3.33$, $\beta=3.76$ for 2.4 mm), (c) sliding/rolling particles ($\alpha=2.93$, $\beta=0.87$ for 2.4 mm).

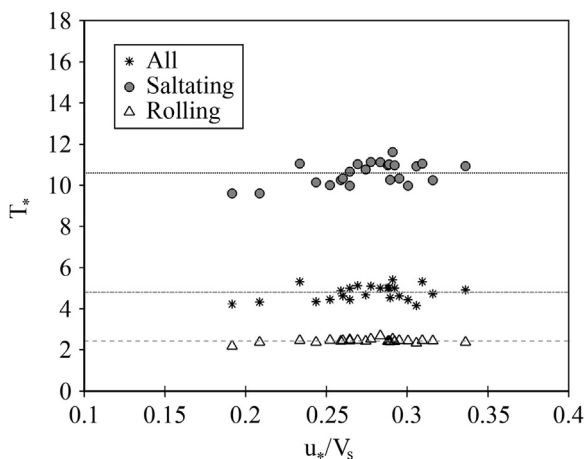


Fig. 10. Dimensionless travel time, each horizontal line represents a linear fit of each data set.

4.4. Averaged velocity of particles

In addition to the instantaneous velocity measured using two consecutive images, the averaged velocity of all the moving particles were also calculated. Those velocities were calculated by dividing the travel distance of each particle in a continuous motion by the travel time. The average particle velocity is the average of all the velocities of moving particles at a given flow condition, which is plotted versus the friction velocity in Fig. 11. When u_*/V_s is smaller than 0.25, \bar{u}_p/V_s ranges from 0.78 to 0.85, but when u_*/V_s is larger than 0.25, it increases linearly with u_*/V_s .

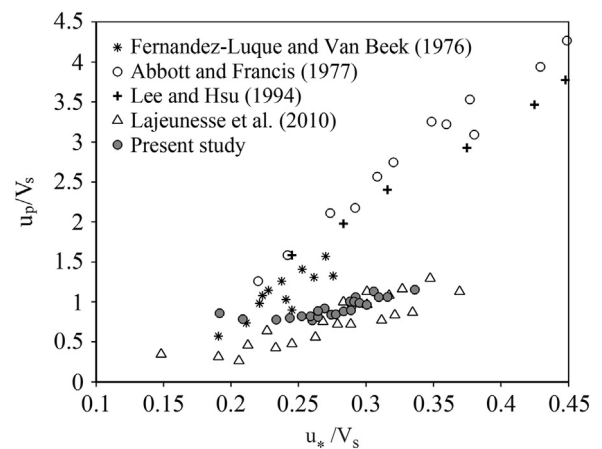


Fig. 11. Average particle velocity, \bar{u}_p/V_s , versus u_*/V_s .

The velocity measurements were also compared with data from previous studies. Two different trends are visible depending on the nature of bed surface and the mode of particle motion. For a single particle above a fixed bed (Abbott & Francis, 1977; Lee & Hsu, 1994) or selective particle motions above an erodible bed (Fernandez Luque & Van Beek, 1976), the particle velocities were larger than those obtained by averaging over all measurements on mobile bed. It's apparent that a single or a few selected particles are not sufficient to represent the particle velocity over a mobile bed in this study. The interactions between particles impose a resistance force to decelerate the moving particles. Furthermore, as sediment particles are transported as a group on a mobile bed surface, the particle velocities are varying with particle sizes,

shapes, and placements. When all the moving particles are taken into account, the averaged particle velocity should be smaller than those using a single or a few selected particles. Lajeunesse et al. (2010) also conducted experiments to record the velocities of all the moving particles, and found a similar linear relation, but slightly smaller values than those in the present study for $u_* / V_s < 0.25$. This may be attributed to the fact that the study by Lajeunesse et al. (2010) used a larger sized particle.

5. Sediment transport rate

Bed load sediment transport rate is the sum of the product of each transported particle's volume and its velocity in the streamwise direction. The diameter of each particle is approximated by the equivalent diameter for the area enclosed by its contour, in which $D_i = \sqrt{4A_i/\pi}$, where A_i is the area of the i th contour. The volume of a particle can be calculated as:

$$V_i = \frac{1}{6}\pi D_i^3 \quad (18)$$

where V_i is the volume of the i th particle at each frame. Sediment transport rate in mass per unit width and time is given by

$$q_{bj} = \frac{\sum_{i=1}^n \rho_s V_i u_{pi}}{A_s} \quad (19)$$

$$q_b = \frac{1}{N} \sum_{j=1}^N q_{bj} \quad (20)$$

where q_{bj} is the instantaneous bed load transport rate at the j th frame, n is the total number of particle moving in j th frame; N is the number of total frames; ρ_s is the density of sediment, u_{pi} is the instantaneous particle velocity for i th particle, A_s is the area covered in the image, and q_b is the averaged bed-load transport rate over N frames. The physical samples of bed-load sediment were collected in 20 gallon basket at the end of the flume for 1.0 min during each run to verify the accuracy of the image-based calculations. Physically measured bed load transport rate was determined using the weight of sediment per unit time per unit width of the flume. A total of 29 bed load measurements were obtained. The bed-load transport rates calculated by Eq. (20) were compared with the manually measured ones, as shown in Fig. 12. The results indicated that the mean error of Eq. (20) for calculating bed load transport rate is 5%. This result implies that the particle tracking method developed in this study is capable of measuring all the moving particles' velocities accurately regardless of sliding, rolling, or saltation motions.

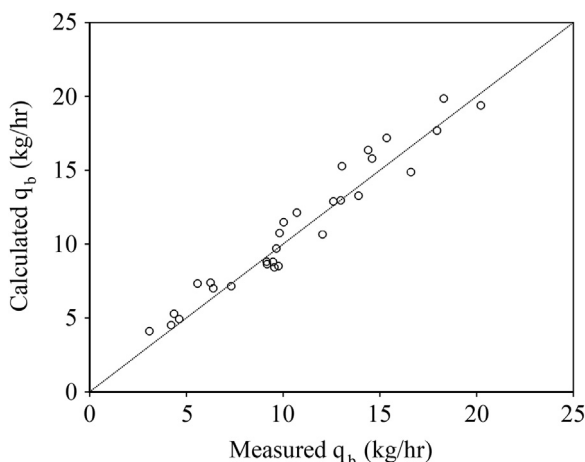


Fig. 12. Calculated sediment transport rate versus manually measured sediment transport rate.

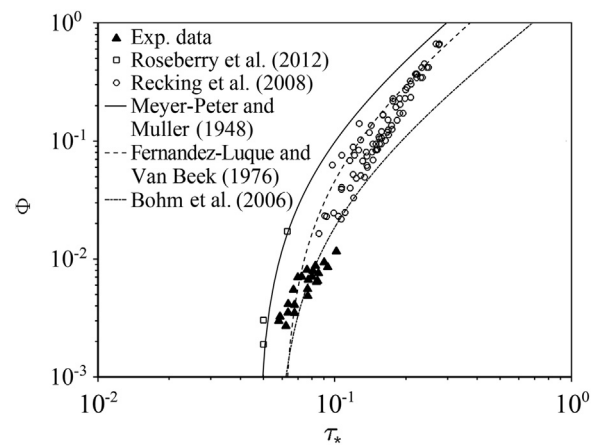


Fig. 13. Dimensionless transport rate versus Shields number; the experiment data by Recking et al. (2008) and Roseberry et al. (2012), semi-empirical formulas (lines) provided by Meyer-Peter and Muller (1948), Fernandez Luque and van Beek (1976) and Bohm et al. (2006).

Bed-load transport rate, calculated using the particle tracking method is presented in Fig. 13 along with data from previous researches (Recking et al., 2008; Roseberry et al., 2012). Each transport rate from this study was calculated using 1398 images obtained in 16 s. The dimensionless bed load transport rate is defined in Eq. (5). Three empirical sediment transport formulas were also plotted: the Meyer-Peter–Muller formula (Meyer-Peter & Muller, 1948) $\Phi = 8(\tau_* - 0.047)^{3/2}$, the Fernandez Luque and Van Beek formula (Fernandez Luque & Van Beek, 1976) $\Phi = 5.7(\tau_* - 0.06)^{3/2}$, and Bohm formula (Bohm et al., 2006). The measured bed load transport rate using the particle tracking technique in this study were within the range of all three bed load transport equations. The match of our experimental results with these three formulas, as well as experimental and field data indicates that the particle tracking method will potentially enable the image based automation of bed load transport measurement. However, experimental data from this study have low shear stress. Additional data of particle velocity at high transport rate are needed to further verify this particle tracking method.

6. Conclusions

This study developed a particle tracking method that is able to automatically identify moving particles, match them in consecutive images, and automatically compute particle velocity and bed load transport rate. Results showed that our particle tracking algorithm can automatically distinguish multiple moving particles in each frame and track the motion of each particle on a mobile bed surface. Using this result, high levels of accuracy were achieved for the measurement of bed load transport rate and particle velocity when saltating and rolling/sliding motions occur simultaneously.

In addition, the travel length and time of all the moving particles were empirically correlated with flow shear velocity. The results indicate the travel length is nearly a constant at low shear velocity ($u_* / V_s < 0.25$), when sliding/rolling motion was dominant. However, when the shear velocity is greater than 0.25, the travel length increases rapidly. Bed-load transport rate measured by using the particle tracking method was compared with the manually measured ones. The results confirmed that the particle tracking method presented in this paper made it possible to measure bed load transport rate at the individual particle scale, including the spatial and temporal variations of bed load transport rate. However, the experimental data was limited to uniform sized

sediment with the particle Reynolds numbers ranging from 90 to 150. And our experimental data are only limited to particle transport at low shear stress, we expect that this method will be applicable to flows with high sediment transport rate by using cameras with a sampling frequency of 200–500 Hz. Our ultimate goal is to apply this particle tracking method to natural rivers. In the future, we will collect field data using this technique to further verify its applicability.

References

- Abbott, J. E., & Francis, J. R. D. (1977). Saltation and suspension trajectories of solid grains in a water stream. *Philosophical Transactions of the Royal Society of London Series A*, 284(1321), 225–254.
- Ancey, C., & Heyman, J. (2014). A microstructural approach to bed load transport: Mean behaviour and fluctuations of particle transport rates. *Journal of Fluid Mechanics*, 744, 129–168. <http://dx.doi.org/10.1017/jfm.2014.74>.
- Bagnold, R. A. (1973). Nature of saltation and of bed-load transport in water. *Proceedings of the Royal Society of London Series A*, 332(1591), 473–504. <http://dx.doi.org/10.1098/rspa.1973.0038>.
- Bohm, T., Frey, P., Ducottet, C., Ancey, C., Jodeau, M., & Reboud, J. L. (2006). Two-dimensional motion of a set of particles in a free surface flow with image processing. *Experiments in Fluids*, 41(1), 1–11. <http://dx.doi.org/10.1007/s00348-006-0134-9>.
- Bradski, G., & Kaehler, A. (2008). In: M. Loukides (Ed.), *Learning OpenCV* (1st ed.). Sebastopol, CA: O'Reilly.
- Bridge, J. S., & Dominic, D. F. (1984). Bed load grain velocities and sediment transport rates. *Water Resources Research*, 20(4), 476–490. <http://dx.doi.org/10.1029/Wr020i004p00476>.
- Buffington, J. M., & Montgomery, D. R. (1997). A systematic analysis of eight decades of incipient motion studies, with special reference to gravel-bedded rivers. *Water Resources Research*, 33(8), 1993–2029. <http://dx.doi.org/10.1029/96wr03190>.
- Campagnol, J., Radice, A., Nokes, R., Bulankina, V., Lescova, A., & Ballio, F. (2013). Lagrangian analysis of bed-load sediment motion: Database contribution. *Journal of Hydraulic Engineering*, 51(5), 589–596. <http://dx.doi.org/10.1080/00221686.2013.812152>.
- Drake, T. G., Shreve, R. L., Dietrich, W. E., Whiting, P. J., & Leopold, L. B. (1988). Bedload transport of fine gravel observed by motion-picture photography. *Journal of Fluid Mechanics*, 192, 193–217. <http://dx.doi.org/10.1017/s0022112088001831>.
- Fernandez Luque, R., & Van Beek, R. (1976). Erosion and transport of bed-load sediment. *Journal of Hydraulic Research*, 14(2), 127–144. <http://dx.doi.org/10.1080/00221687609499677>.
- Francis, J. R. D. (1973). Experiments on the motion of solitary grains along the bed of a water-stream. *Proceedings of the Royal Society of London Series A*, 332(1591), 443–471.
- Frey, P. (2014). Particle velocity and concentration profiles in bedload experiments on a steep slope. *Earth Surface Processes and Landforms*, 39(5), 646–655. <http://dx.doi.org/10.1002/esp.3517>.
- Furbish, D. J., Roseberry, J. C., & Schmeeckle, M. W. (2012). A probabilistic description of the bed load sediment flux: 3. The particle velocity distribution and the diffusive flux. *Journal of Geophysical Research-Earth Surface*, 117, F03033. <http://dx.doi.org/10.1029/2012jf002355>.
- Furbish, D. J., & Schmeeckle, M. W. (2013). A probabilistic derivation of the exponential-like distribution of bed load particle velocities. *Water Resources Research*, 49(3), 1537–1551. <http://dx.doi.org/10.1002/wrcr.20074>.
- Heays, K. G., Friedrich, H., Melville, B. W., & Nokes, R. (2014). Quantifying the dynamic evolution of graded gravel beds using particle tracking velocimetry. *Journal of Hydraulic Engineering*, 140(7), 04014027. [http://dx.doi.org/10.1061/\(asce\)hy.1943-7900.0000850](http://dx.doi.org/10.1061/(asce)hy.1943-7900.0000850).
- Houssais, M., & Lajeunesse, E. (2012). Bedload transport of a bimodal sediment bed. *Journal of Geophysical Research*, 117, F04015. <http://dx.doi.org/10.1029/2012jf002490>.
- Julien, P. Y., & Bounvilay, B. (2013). Velocity of rolling bed load particles. *Journal of Hydraulic Engineering*, 139(2), 177–186. [http://dx.doi.org/10.1061/\(asce\)hy.1943-7900.0000657](http://dx.doi.org/10.1061/(asce)hy.1943-7900.0000657).
- Laganier, R. (2011). *OpenCV 2 Computer vision application programming cookbook*. Birmingham, UK: Packt Publishing Ltd.
- Lajeunesse, E., Malverti, L., & Charru, F. (2010). Bed load transport in turbulent flow at the grain scale: Experiments and modeling. *Journal of Geophysical Research*, 115, F04001. <http://dx.doi.org/10.1029/2009jf001628>.
- Le Roux, J. P. (2004). An integrated law of the wall for hydrodynamically transitional flow over plane beds. *Sedimentary Geology*, 163(3–4), 311–321. <http://dx.doi.org/10.1016/j.sedgeo.2003.07.005>.
- Lee, H. Y., & Hsu, I. S. (1994). Investigation of saltating particle motions. *Journal of Hydraulic Engineering*, 120(7), 831–845.
- Meyer-Peter, E., & Muller, R. (1948). Formulas for bed-load transport. *Paper presented at the International Assoc. Hydraul. Res.*, Stockholm, Sweden.
- Niño, Y., & García, M., H. (1994a). Gravel saltation 1. experiments. *Water Resources Research*, 30(6), 1907–1914.
- Niño, Y., & García, M., H. (1994b). Gravel saltation 2. modeling. *Water Resources Research*, 30(6), 1915–1924.
- Niño, Y., & García, M., H. (1998). Experiments on saltation of sand in water. *Journal of Hydraulic Engineering*, 124(10), 1014–1025.
- Novak, P., & Nalluri, C. (1975). Sediment transport in smooth fixed-bed channels. *Journal of the Hydraulics Division*, 101(9), 1139–1154.
- Papanicolaou, A. N., Diplas, P., Balakrishnan, M., & Dancy, C. (1999). Computer vision technique for tracking bed load movement. *Journal of Computing in Civil Engineering*, 13(2), 71–79. [http://dx.doi.org/10.1061/\(ASCE\)0887-3801\(1999\)13:2\(71\)](http://dx.doi.org/10.1061/(ASCE)0887-3801(1999)13:2(71)).
- Papanicolaou, A.N., Knapp, D., & Strom, K. (2002). Bedload predictions by the using concept of particle velocity: applications. *Paper presented at the EWRI International conf. on Hydraulic Measurements and Experimental Methods*, Estes Park, Colorado.
- Parker, G. (2008). Transport of gravel and sediment mixtures In: M. Garcia (Ed.), *Sedimentation engineering: processes, measurements, modelling and practice* (pp. 165–251). ASCE.
- Radice, A., Malavasi, S., & Ballio, F. (2006). Solid transport measurements through image processing. *Experiments in Fluids*, 41(5), 721–734. <http://dx.doi.org/10.1007/s00348-006-0195-9>.
- Ramesh, B., Kothiyari, U. C., & Murugesan, K. (2011). Near-bed particle motion over transitionally-rough bed. *Journal of Hydraulic Research*, 49(6), 757–765. <http://dx.doi.org/10.1080/00221686.2011.620369>.
- Recking, A., Frey, P., Paquier, A., Belleudy, P., & Champagne, J. Y. (2008). Bed-load transport flume experiments on steep slopes. *Journal of Hydraulic Engineering*, 134(9), 1302–1310. [http://dx.doi.org/10.1061/\(asce\)0733-9429\(2008\)134:9\(1302\)](http://dx.doi.org/10.1061/(asce)0733-9429(2008)134:9(1302)).
- Roseberry, J. C., Schmeeckle, M. W., & Furbish, D. J. (2012). A probabilistic description of the bed load sediment flux: 2. Particle activity and motions. *Journal of Geophysical Research-Earth Surface*, 117, F03032. <http://dx.doi.org/10.1029/2012jf002353>.
- Sekine, M., & Kikkawa, H. (1992). Mechanics of saltating grains. *Journal of Hydraulic Engineering*, 118(4), 536–558.
- Tregnaghi, M., Bottacin-Busolin, A., Marion, A., & Tait, S. (2012a). Stochastic determination of entrainment risk in uniformly sized sediment beds at low transport stages: 1. Theory. *Journal of Geophysical Research-Earth Surface*, 117, F04004. <http://dx.doi.org/10.1029/2011jf002134>.
- Wu, F. C., & Yang, K. H. (2004). A stochastic partial transport model for mixed-size sediment: Application to assessment of fractional mobility. *Water Resources Research*, 40(4), W04501. <http://dx.doi.org/10.1029/2003wr002256>.